Ultrasonics Sonochemistry 82 (2022) 105913

Contents lists available at ScienceDirect

Ultrasonics Sonochemistry

journal homepage: www.elsevier.com/locate/ultson

High-intensity ultrasound promoted the aldol-type condensation as an alternative mean of synthesizing pyrazines in a Maillard reaction model system of D-glucose-$^{13}C_6$ and L-glycine

Ruyue Zhang [a,b,c,d], Yilong Zhang [a,b,c,d], Yating Sun [a,b,c,d], Hang Yu [a,b,c,d,*], Fangwei Yang [a,b,c,d], Yahui Guo [a,b,c,d], Yunfei Xie [a,b,c,d], Weirong Yao [a,b,c,d]

[a] State Key Laboratory of Food Science and Technology, Jiangnan University, 1800 Lihu Avenue, Wuxi, Jiangsu Province 214122, China
[b] School of Food Science and Technology, Jiangnan University, 1800 Lihu Avenue, Wuxi, Jiangsu Province 214122, China
[c] Joint International Research Laboratory of Food Safety, Jiangnan University, No.1800 Lihu Avenue, Wuxi, Jiangsu Province 214122, China
[d] Collaborative Innovation Center of Food Safety and Quality Control in Jiangsu Province, Jiangnan University, 1800 Lihu Avenue, Wuxi, Jiangsu Province 214122, China

ARTICLE INFO

Keywords:
Ultrasound
Aldol-type condensation
Maillard reaction
Pyrazine
Carbon module labeling
Glucose
Glycine

ABSTRACT

This study evaluated how the generation of pyrazines was promoted by high-intensity ultrasound (HIU) in a Maillard reaction (MR) model system of glucose-glycine. Carbohydrate module labeling (CAMOLA) technique was adopted using D-glucose-$^{13}C_6$ to elucidate the carbon skeleton of both intermediate and final MR products (MRPs). In the D-glucose-$^{13}C_6$-glycine HIU-MR model system, the concentration of 11 types of pyrazines was significantly higher than their counterparts in the thermal MR. Results of CAMOLA analysis showed that a significantly lower proportion of $[M]^+$ in pyrazines with long-length side chains was observed when compared with the pyrazines generated in thermal MR. This phenomenon may suggest the aldol-type condensation was promoted by the HIU, which is a conversion from pyrazines with short-length side chains to those with long-length side chains involving carbonyl compounds. Furthermore, the analysis of isotopomers distribution in 2,3-dimethyl-quinoxaline as the o-phenylenediamine-derivatized 2,3-butanedione indicated that the increased proportion of $[M + 4]^+$ in 2,3-dimethyl-quinoxaline (15.74% ± 0.11%) was attributed to a cleavage of D-glucose-$^{13}C_6$ promoted by the HIU. The above-mentioned findings elucidate that the aldol-type condensation and cleavage of D-glucose contribute to the promoted synthesis of pyrazines. The HIU would generate an extremely high temperature and pressure environment that is favored by the aldol-type condensation as a high-pressure favored reaction. The HIU, therefore, can be further developed as a promising technique to promote flavor generation through the MR.

1. Introduction

Pyrazines are a group of heterocyclic compounds with strong flavoring impacts in food products. In general, pyrazines provide characteristic sensory impacts that are normally described as desirable roasted, baking, nutty flavors, etc. [1]. During the thermal treatment of foods, pyrazines are normally generated through Maillard reaction (MR) that is involved reducing sugars and amino acids/peptides/proteins [2]. In general, the Strecker degradation at the final stage of MR mainly contributes to synthesizing the pyrazines. However, the extent of Strecker degradation is relatively low that normally has a high value of activation energy (E_a) [3]. Meanwhile, its corresponding precursors are generally unstable and the content of some intermediate MR products (MRPs) is relatively low, such as 1-deoxyglucosone (1-DG), 3-deoxyglucosone (3-DG), methylglyoxal (MG), glyoxal (GO), etc. Furthermore, the α-dicarbonyl compounds are possibly involved in many other reactions and therefore, only partial α-dicarbonyl compounds are involved in the synthesize of pyrazines [4,5]. Due to these reasons, it is necessary to develop a new technique to promote the MR and thereby synthesize more pyrazines with better quality. This technique could be also adopted to enhance food flavors and properties via MR during food processing [6].

Among emerging technologies, high-intensity ultrasound (HIU) has been proved to significantly promote MR and more importantly,

* Corresponding author at: State Key Laboratory of Food Science and Technology, Jiangnan University, 1800 Lihu Avenue, Wuxi, Jiangsu Province 214122, China.
E-mail address: hangyu@jiangnan.edu.cn (H. Yu).

https://doi.org/10.1016/j.ultsonch.2022.105913
Received 29 October 2021; Received in revised form 11 December 2021; Accepted 8 January 2022
Available online 11 January 2022

synthesize higher content and more types of flavor compounds [7]. Starting from the year 2010, Guan, Wang, Yu, Xu and Zhu [8] evaluated the impacts of HIU at different intensity levels on a glycine-maltose MR model system. The HIU at the intensity of 17.83 W/cm^2 for 100 min significantly promoted the MR to generate MRPs with a higher antioxidant capacity. Another follow-up study in a MR model system consisting of glucose and glycine observed that the production of flavor compounds was promoted with the assistance of HIU at the same intensity level, including trimethyl pyrazine, 2,5-dimethyl pyrazine, (Z)-9-octadecenamide, etc. [9]. More progress on the HIU-assisted MR (HIU-MR) have been made in recent years. For example, the generation of 2-methyl thiophene and tetramethyl pyrazine was optimized in the HIU-MR model system consisting of xylose and cysteine [10]. There was a similar finding reported in an HIU-MR model system containing methionine and glucose, which reported a promoted generation of methional and 2,5-dimethyl pyrazine [11]. Results of both studies indicated that not only nitrogen-containing but also sulfur-containing odor-active MRPs could be promoted with the assistance of HIU. Yu, Seow, Ong and Zhou [3] utilized multi-response kinetic modeling to reveal key reaction steps that were significantly promoted by HIU in a MR model system of glucose-glycine. There were two generation pathways, i.e. 1-DG and 3-DG as precursors of pyrazines, that required more than 40% less of E_a compared with those in thermal MR. The Strecker degradation as a key step to synthesize pyrazines was promoted as well, which required 11.12% to 25.85% less of E_a to synthesize 2,3,5-trimethyl pyrazine, 2,5-dimethyl pyrazine, tetramethyl pyrazine, and 3-ethyl-2,5-dimethyl pyrazine compared with those in thermal MR. It is noticeable that 3,5-diethyl-2-methyl pyrazine, and 2-vinyl-3,5-dimethyl pyrazine were only synthesized in the HIU-MR instead of the thermal MR. These phenomena were attributed to a favorable high temperature and pressure environment generated by HIU that promoted the formation of two pyrazines.

Although almost all the previous studies have observed the promoted generation of pyrazines as a common phenomenon, there is no insight into the generation mechanisms of pyrazines. In addition, the question remained uncertain whether the HIU treatment would alert the reaction pathway to generate those unique pyrazines in the HIU-MR model system. To further elucidate generation mechanisms, the carbon module labeling (CAMOLA) technique was adopted as a powerful tool to elucidate the carbon skeleton of the MRPs and therefore, clarify the pathway of pyrazines generation in the HIU-MR model system. The CAMOLA technique is capable of identifying the origins of ^{13}C-labeled atom to further speculate potential generation pathways through the analysis of ^{13}C-labeled final MRPs and their corresponding precursors [12]. For instance, the CAMOLA technique was utilized in a 1,4-^{13}C-labeled ascorbic acid and glutamic acid MR model system. It was successfully determined that C-4 in ascorbic acid participated in the generation of pyrazines instead of C-1. Furthermore, several active intermediates, such as acetol, butanedione, and hydroxy butadione, were pyrolyzed from ascorbic acid in the MR model system; these intermediate MRPs subsequently reacted with the ammonia as a degradation product of glutamic acid to synthesize α-amino carbonyl or α-amino hydroxy compounds as precursors of pyrazines [13,14]. Another study on a MR model system that involved alanine-leucine dipeptide and xylose has identified 7 new Amadori-type conjugates followed by elucidating their roles in the formation of pyrazines. It was summarized that these Amadori-type conjugates significantly influenced the quantities and ratios of pyrazines [15].

In the present study, a MR model system of L-glycine and equal molar of D-glucose-$^{13}C_6$ and unlabeled glucose was chosen to study the effects of HIU on the generation mechanisms of pyrazines. The CAMOLA technique was utilized to analyze differences in the carbon skeleton of the pyrazines and their corresponding precursors. Based on these results, a systematic reaction scheme of the HIU-MR model system with glucose and glycine was established. Meanwhile, potential reaction pathways were proposed to elucidate how the generation of pyrazines was promoted by the HIU.

2. Materials and methods

2.1. Preparation of Maillard reaction model system

The chemicals in this study included glycine (≥99.0%), sodium chloride (≥99.0%), D-glucose (≥99.0%), and o-phenylenediamine (OPD) (≥98.0%), which were purchased from Aladdin (Shanghai, China). In addition, D-glucose-$^{13}C_6$ (≥99.0%) was purchased from Sigma-Aldrich. Equal amounts (0.05 mol) of labeled and unlabeled D-glucose combined with glycine (0.1 mol) were dissolved in 100 mL of deionized water. The pH of the sample solution was adjusted to 10.0 by adding sodium hydroxide.

2.2. High-intensity ultrasound (HIU) treatment

An ultrasound system (UIP 500, Hielscher, Germany) was chosen to conduct high-intensity ultrasonic treatment. Twelve mL of the reaction solution was transferred into a 50 mL bioreactor. A rubber plug was sealed at the top of bioreactor; a titanium ultrasonic probe with a frontal diameter of 22 mm (BS2d22, Hielscher, Germany) was inserted into the bioreactor. The distance between the ultrasonic probe and the bottom of the bioreactor was kept constant at 10 mm. Cooling water was kept pumping through a water jacket outside the bioreactor. The temperature of ultrasound treatment was maintained at 95℃. The output power of ultrasound was set to 90 W and the intensity was calculated to be 23.69 W/cm^2. The duration of each treatment was 90 min. At the end of the process, the processed sample solution was collected and sealed into a 20 mL headspace bottle followed by immersing in ice water before further tests.

2.3. Thermal treatment

The same bioreactor was used for the thermal MR as described in section 2.2. The reaction temperature was maintained at 95℃ and the duration was 90 min. The processed sample solution was collected and sealed into a 20 mL headspace bottle followed by immersing in ice water before further tests.

2.4. Determination of α-dicarbonyl compounds

2.4.1. Derivatization of α-dicarbonyl compounds

Qualification of α-dicarbonyl compounds was conducted followed by the method described in Yu, Seow, Ong and Zhou [3] with modifications. The sample solution was pre-derivatized by OPD. In brief, a 1.2 mL sample solution was mixed with 0.8 mL of OPD at the concentration of 10 mg/mL in methanol. The pH value of mixture was adjusted to 12.0 with the addition of sodium hydroxide. Subsequently, 8 mL of ethyl acetate was added to the mixture and then extracted the derivatized α-dicarbonyl compounds using a magnetic stirrer (RCT B S025, IKA, Germany) at 900 rpm for 5 min. The extract was then centrifuged (TGL-16 M, Bioridge, China) at 1,240 g at 4℃ for 10 min. Two μL of supernatant was collected and injected into the inlet of GCMS for further analysis.

2.4.2. GCMS analysis of α-dicarbonyl compounds

A GCMS system (GC-HRT 4D+, LECO Pegasus, US) equipped with a DB-Wax column (30 m × 0.25 mm × 0.25 μm, J &W Scientific, US) was adopted to separate the α-dicarbonyl compounds. Helium and nitrogen were used as the carrier gas (1.5 mL/min) and make-up gas (5 mL/min), respectively. The spitless injection mode was chosen at 250℃. The oven program was set as follows: the initial temperature was set to 40℃ and maintained for 2 min. The oven temperature was then raised to 230℃ at 20℃/min followed by maintaining the temperature for 6 min at 230℃ until the end of analysis. The GCMS transfer line temperature was

Table 1
Summary of volatile MPRs detected in both HIU-MR and thermal MR model system of glucose-glycine.

Classification	Volatile MRPs	Retention indices[1]		Concentration (μg/L)	
		Measured	Documented	HIU-MR	Thermal MR
Alcohols	Heptanol	1454	1457	1.16	—[2]
	2-ethyl-1-Hexanol	1488	1484	2.13	1.48
	1-Octanol	1556	1561	3.24	0.12
	Acetone alcohol	1309	1290	0.99	0.07
	5-methyl-2-Furanmethanol	1727	1720	10.91	—
Aldehydes	Hexanal	1084	1078	1.23	1.31
	Heptanal	1188	1181	2.35	0.34
	Benzaldehyde	1538	1529	19.09	3.61
	Nonanal	1397	1397	1.66	0.78
Ketones	2-Heptanone	1185	1184	182.32	178.99
	2-Octanone	1288	1297	39.56	0.04
	2,3-Pentanedione	1065	1062	18.38	0.18
	Acetoin	1289	1285	0.40	0.05
	Acetophenone	1666	1652	1.21	0.27
	Benzophenone	2507	2470	4.65	1.39
	(E)-6,10-dimethyl-5,9-Undecadien-2-one	1861	1862	5.65	1.76
	1-(1-methyl-1H-pyrrol-2-yl)- Ethanone	1669	1647	3.43	0.17
	1-(1H-pyrrol-2-yl)- Ethanone	1984	1980	7.57	0.18
	1-(2-pyridinyl)- Ethanone	1617	1602	5.61	0.14
Esters	ethyl Acetate	897	887	23.43	6.61
	2,2,4-trimethyl-1,3-Pentanediol diisobutyrate	1881	1882	11.53	0.94
	Diethyl Phthalate	2386	2401	47.25	0.58
Pyrazines (heterocyclic compounds)	2-methyl Pyrazine	1271	1264	157.89	116.02
	2,6-dimethyl Pyrazine	1333	1338	0.23	—
	2,5-dimethyl Pyrazine	1326	1316	3.37	1.19
	2,3-dimethyl Pyrazine	1352	1346	1194.77	29.70
	2-ethyl-6-methyl Pyrazine	1389	1393	534.00	325.01
	2-ethyl-5-methyl Pyrazine	1396	1399	1417.59	495.58
	2,3,5-trimethyl Pyrazine	1409	1408	154.44	122.55
	3-ethyl-2,5-dimethyl Pyrazine	1449	1455	32.96	3.53
	2-ethyl-3,5-dimethyl Pyrazine	1466	1467	9.57	0.63
	tetramethyl Pyrazine	1479	1478	733.77	895.12
	3,5-diethyl-2-methyl Pyrazine	1517	1503	0.48	0.07
	2-vinyl-3,5-dimethyl-Pyrazine	1547	1547	25.47	8.07
The rest of heterocyclic compounds	2-methyl Furan	876	877	207.45	30.73
	2-acetyl-5-methyl Furan	1624	1624	1.28	4.23
	2-formyl Pyrrole	2041	2036	4.11	1.80
	2-methyl Pyridine	1223	1227	4.15	5.61
	Quinoxaline	1929	1879	3.22	10.37
	Quinoline	1960	1942	7.65	6.15
	5-methyl Quinoxaline	2051	2051	0.44	0.31
	Phenol	2014	2010	1.09	0.44

[1] Retention indices documented in the National Institute of Standards and Technology (NIST) WebBook Database (https://webbook.nist.gov/chemistry/).
[2] The symbol of "—" refers to not detected.

250℃. Electron-impact mass spectra were generated at 70 eV in an *m/z* scan range from 40 to 500. The mass spectrum source temperature was 210℃. The derivatized compounds were identified and compared their spectra with that in an MS library (mainlib NIST2014).

2.5. Determination of volatile MRPs

For extracting volatile MRPs in the samples of HIU-MR and thermal MR, a triple-phase micro-extraction (SPME) fiber with 50/30 μm divinylbenzene/carboxen (DVB/CX) on poly dimethylsiloxane (PDMS) coating was inserted into a glass vial with the 4 mL processed sample. At the end of a 20 min-extraction, the SPME fiber was injected into the GCMS inlet for further analysis.

The mode of GCMS was the same as described in section 2.3. Internal standard was 2-methyl-3-heptanone. Helium was used as the carrier gas at a flow rate of 1 mL/min. The effluent from the capillary column was split 1:1 (mL/mL) between the mass spectrometry detector and the sniffing port. The initial temperature of GC oven was set to 40℃ and then maintained for 3 min. Subsequently, the oven temperature was increased to 230℃ at a rate of 10℃/min followed by holding at 230℃ for 6 min. The MS conditions were the same as reported in the previous section. The volatile compounds were identified and compared their spectra with that in an MS library (mainlib NIST2014). Retention indices (RI) were obtained from the National Institute of Standards and Technology (NIST) WebBook Database (https://webbook.nist.gov/chemistry/).

2.6. Identifying transient intermediates using CAMOLA technique

The CAMOLA technique was designed to understand the effect of ultrasound-assisted MR on the pyrazine synthesis pathway. Equal molar of D-glucose-$^{13}C_6$ and unlabeled D-glucose was mixed as reactants. The relative isotopic contents in the MRPs were calculated by analyzing the relative signal intensities (*m/z*) of the ions in the high-resolution MS of the respective compounds [15].

2.7. Determination of melanoidins

Absorbance at 420 nm was measured by UV–Vis spectrophotometer (UV–vis 1280, Shimadzu, Japan) as an indicator of melanoidins content in the MRPs. The sample solution was diluted 20 times before the analysis. The concentration of melanoidins was calculated based on the Lambert-Beer law. An extinction coefficient, i.e. 0.60 L/(mmol × cm), was utilized as reported in Kim [16].

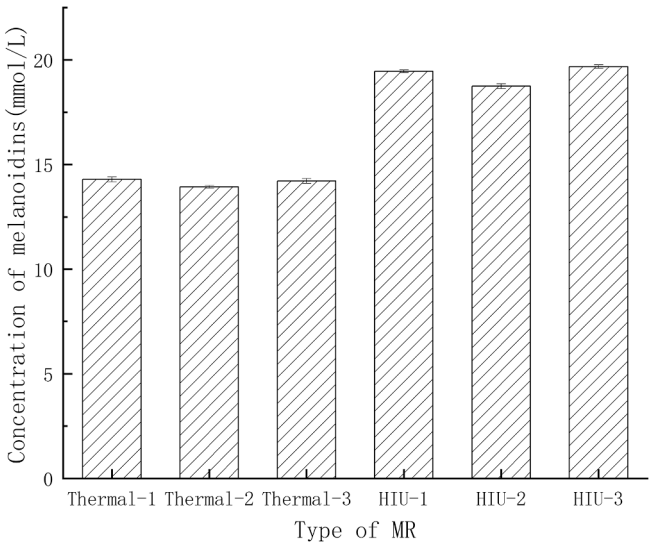

Fig. 1. Concentration of melanoidins generated in HIU-MR and thermal MR model systems of D-glucose-L-glycine.

2.8. Statistical analysis

All data presented in this study was a mean of triplicate. Significant difference test among the data was tested by SPSS (version 20, IBM, US) using one-way analysis of variance (ANOVA) with Duncan's multiple range test ($p < 0.05$).

3. Results and discussion

3.1. Volatile MRPs generated from HIU-MR and thermal MR model systems of D-glucose-L-glycine

Volatile MRPs generated from HIU-MR and thermal MR model systems of D-glucose-L-glycine are summarized in Table 1. The reaction temperature and duration of HIU-MR and thermal MR were 95℃ and 90 min, respectively. For HIU-MR, the power of ultrasound input into the system was 90 W; the intensity level of ultrasound was 23.69 W/cm^2. There were 41 volatile MRPs detected in the HIU-MR, which were four more volatile MRPs in the thermal MR, i.e. heptanol, hexanal, 2,2,4-trimethyl-1,3-pentanediol diisobutyrate, and quinoline. Furthermore, the content of volatile MRPs generated in HIU-MR was relatively higher than those generated in the thermal MR. These results are in accordance with the concentration of melanoidins generated in the two types of MR. For HIU-MR, the concentration of melanoidins (19.29 ± 0.49 mmol/L) was significantly higher than that in the thermal MR (14.14 ± 0.19 mmol/L), which reflected the extent of MR as shown in Fig. 1. The content of pyrazines generated in the HIU-MR was generally higher than those in the thermal counterpart. For example, the peak area of 2-methyl-pyrazine with a short-length of side chain in the HIU-MR was 157.89 μg/L, which was higher than that in the thermally processed sample (116.02 μg/L). Besides the 2-methyl-pyrazine, the concentration of 2,3,5-trimethyl pyrazine in the HIU-MR (154.44 μg/L) was also higher than those in the thermal MR (122.55 μg/L). It is noticeable that the peak area of pyrazines with long-length of side chains in the HIU-MR was about two or more times higher than those in the thermal MR, including 2-ethyl-6-methyl pyrazine, 2-ethyl-5-methyl pyrazine, 3-ethyl-2,5-dimethyl pyrazine, 2-ethyl-3,5-dimethyl pyrazine, 3,5-diethyl-2-methyl pyrazine, and 2-vinyl-3,5-dimethyl-pyrazine. As long as the methyl-groups in the pyrazines were replaced by ethyl-groups, the odor thresholds would be significantly decreased. Such a low odor threshold would give a sufficiently high impact on food flavor with a high commercial value.

It is commonly known that the pyrazines are generated through the Strecker degradation as shown in Fig. 2. In the glucose-glycine MR model system, the initial condensation of the two reactants is initiated to generate *N*-glycosylamine and then convert to Schiff base. The Schiff base is further converted to an Amadori compound, which is N-(1-deoxy-D-fructose-1-yl)-glycine (DFG) in this MR model system. The pH conditions have influences on the hydrolysis of DFG. At a low pH condition, DFG prefers to undergo 1,2-enolization and generated 3-DG; 1-DG is largely formed via 2,3-enolization at a relatively high pH condition. Besides 3-DG and 1-DG, MG and GO are the other two important α-dicarbonyl compounds that are largely formed in the MR model system [17]. The cleavage of 3-DG generates MG and glyceraldehyde. For GO, it mainly comes from the cleavage of glucose directly. As key intermediate MRPs, 3-DG and 1-DG are confirmed as precursors of colored MRPs (i.e. melanoidins) and organic acids (i.e. formic acid and acetic acid) [18–20]. Hydrogen or hydroxyl radical formed during the ultrasound treatment could also attributed to the enhanced formation of organic acids [20]. For pyrazines identified in this study, the majority is generated through a pathway that is known as Strecker degradation [21]. Glycine as the amino source in this MR model system condensates with α-dicarbonyl compounds to generate α-amino ketones. The two α-amino ketones are randomly combined together through a self-condensation to generate pyrazines with different side chains and release a molecule of H_2O [2,22]. Some other α-dicarbonyl compounds, including 2,3-butanedione, 2,3-pentanedionie, and 2-oxobutanal, are precursors of some specific types of pyrazines, such as 2-vinyl-3,5-dimethyl pyrazine, 2-ethyl-3,5-dimethyl pyrazine, 2-ethyl-5-methyl pyrazine, and 2-ethyl-6-methyl pyrazine. There are many other products generated through the Strecker degradation (e.g. Strecker aldehydes, oxazoles, thiazoles, etc.) and some carbonyl compounds generated through intermediate MRPs; these MRPs also provide distinctive flavors in the MR [23].

Results of pyrazines generation in the HIU-MR may indicate potential generation/transformation pathways since a significant difference in the concentration of pyrazines with relatively long-length side chains in the HIU-MR and thermal MR, i.e. 2-ethyl-6-methyl pyrazine, 2-ethyl-3,5-dimethyl pyrazine, trimethyl pyrazine, and 2-vinyl-3,5-dimethyl pyrazine. According to Hill, Isaacs, Ledward and Ames [24], although high hydrostatic pressure significantly inhibited the total amount of pyrazines generated in a MR model system of glucose-lysine, a higher content of pyrazines with long-length side chains was observed compared with that in the thermal control. This phenomenon is attributed to a pressure-favored reaction, namely aldol-type condensation [19]. To further confirm the aldol-type condensation as a potential transformation pathway that starts from pyrazines with short-length side chains and various aldehydes to generate the pyrazines with long-length side chains, the CAMOLA technique was adopted to label half of D-glucose-$^{13}C_6$ and further react with L-glycine. Results of isotopic distribution in OPD-derivatized α-dicarbonyl compounds and pyrazines would identify origins of the ^{13}C-labeled atom and further speculate potential generation pathway. These contents are to be discussed in the following section.

3.2. Isotopomers generated from HIU-MR and thermal MR model systems of D-glucose-$^{13}C_6$ and L-glycine

3.2.1. Isotopomers in pyrazines

The proportion of isotopomers in pyrazines is summarized in Table 2. The mass signal fragments of D-glucose-$^{13}C_6$ shown as $[M]^+$ to $[M+9]^+$ were compared with the unlabeled compounds. There were six pyrazines that showed a similar isotopic distribution generated in both HIU-MR and thermal-MR model systems, including 2,5-dimethyl pyrazine, 2,3-dimethyl pyrazine, trimethyl pyrazine, 3-ethyl-2,5-dimethyl pyrazine, tetramethyl pyrazine, 3,5-diethyl-2-methyl pyrazine. A similar isotopic distribution may indicate that these pyrazines originated from the same carbon skeleton [15].

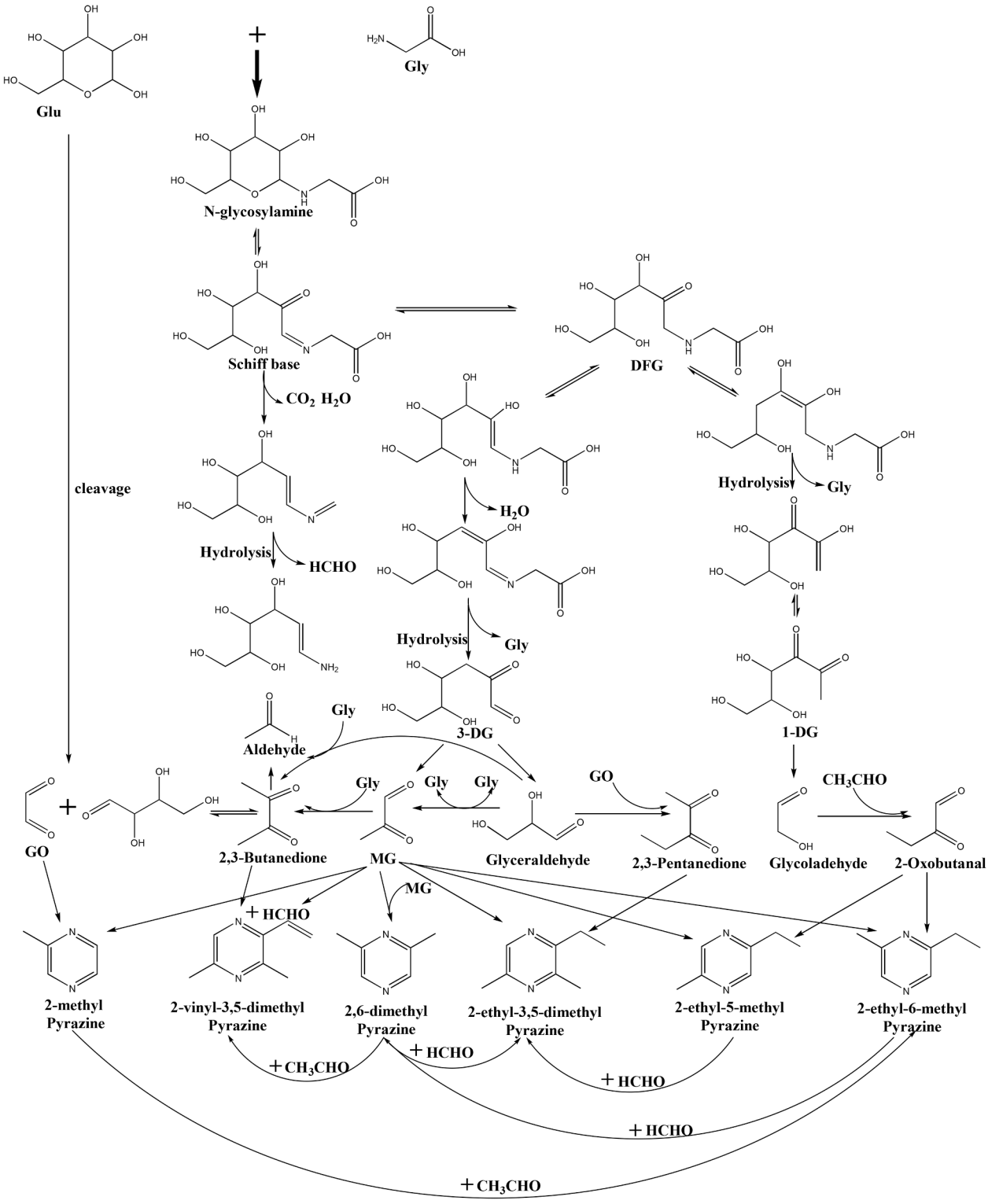

Fig. 2. Reaction scheme of D-glucose-L-glycine HIU-MR model system.

The rest of pyrazines had a different distribution of isotopomers. In general, the proportion of $[M]^+$ in the pyrazines generated in HIU-MR was significantly lower than that in thermal MR. For instance, the proportion of $[M]^+$ in 2-methyl pyrazine was 21.96% ± 0.08% in the sample treated by HIU, which was significantly lower than that in thermal MR (23.44% ± 0.38%). Similarly, the proportion of $[M]^+$ in 2,6-dimethyl pyrazine was 19.95% ± 0.06% in the sample treated by HIU, which was significantly lower than that in thermal MR (21.23% ± 0.20%). In addition, the proportion of $[M]^+$ in 2-ethyl-5-methyl pyrazine was 11.43% ± 0.08% in the sample treated by HIU, which was significantly lower than that in thermal MR (12.23 ± 0.10%). Except for $[M]^+$ proportion in the three pyrazines with short, the proportion of the rest isotopomers had no significant difference between HIU-MR and thermal MR. Looking at the ratio of isotopomers, 2-methyl pyrazine, 2,6-dimethyl pyrazine, and 2-ethyl-5-methyl pyrazine were mainly generated through the condensation of α-amino ketones that came from

Table 2
Proportion of isotopomers in pyrazines generated from D-glucose-$^{13}C_6$ and L-glycine MR model systems with the assistance of HIU and thermal treatment.

Pyrazines	Type of MR	*m/z*	Proportion of labeled carbon atoms in the molecules (%)									
			M	M + 1	M + 2	M + 3	M + 4	M + 5	M + 6	M + 7	M + 8	M + 9
2-methyl Pyrazine	Thermal MR	94.0525	23.44 ± 0.38 [a,1]	4.50 ± 0.11 [a]	27.04 ± 0.43 [a]	21.16 ± 0.24 [a]	6.97 ± 0.09 [a]	16.87 ± 0.35 [a]	—[2]	—	—	—
	HIU-MR		21.96 ± 0.08[b]	4.79 ± 0.02 [a]	28.47 ± 0.10[b]	20.41 ± 0.06[b]	8.14 ± 0.01[b]	16.20 ± 0.01 [a]	—	—	—	—
2,5-dimethyl Pyrazine	Thermal MR	108.0682	21.54 ± 0.91 [a]	3.01 ± 0.09 [a]	5.82 ± 0.07 [a]	41.32 ± 0.12 [a]	3.25 ± 0.03 [a]	4.50 ± 0.18 [a]	20.55 ± 0.84 [a]	—	—	—
	HIU-MR		21.63 ± 0.36 [a]	2.83 ± 0.04 [a]	5.77 ± 0.09 [a]	41.65 ± 0.14 [a]	3.05 ± 0.03[b]	4.25 ± 0.08 [a]	20.79 ± 0.49 [a]	—	—	—
2,6-dimethyl Pyrazine	Thermal MR	108.0682	21.23 ± 0.20 [a]	4.64 ± 0.85 [a]	8.54 ± 1.38 [a]	37.93 ± 1.78 [a]	4.73 ± 0.76 [a]	6.25 ± 0.90 [a]	16.66 ± 1.96 [a]	—	—	—
	HIU-MR		19.95 ± 0.06[b]	6.02 ± 0.13 [a]	11.12 ± 0.42 [a]	34.59 ± 0.55 [a]	6.27 ± 0.14 [a]	8.11 ± 0.35 [a]	13.92 ± 0.43 [a]	—	—	—
2,3-dimethyl Pyrazine	Thermal MR	108.0682	15.66 ± 0.11 [a]	11.03 ± 0.23 [a]	16.97 ± 0.09 [a]	23.76 ± 0.00 [a]	11.28 ± 0.04 [a]	13.39 ± 0.25 [a]	7.88 ± 0.02 [a]	—	—	—
	HIU-MR		15.76 ± 0.09 [a]	10.26 ± 0.18 [a]	17.18 ± 0.11 [a]	23.76 ± 0.04 [a]	10.80 ± 0.15[b]	14.48 ± 0.22[b]	7.73 ± 0.08 [a]	—	—	—
2-ethyl-6-methyl Pyrazine	Thermal MR	122.0838	10.88 ± 0.16 [a]	12.25 ± 0.37 [a]	18.45 ± 0.56 [a]	21.42 ± 0.43 [a]	15.50 ± 0.28 [a]	8.88 ± 0.28 [a]	9.21 ± 0.51 [a]	3.38 ± 0.06 [a]	—	—
	HIU-MR		10.23 ± 0.07[b]	12.26 ± 0.34 [a]	19.70 ± 0.57 [a]	21.09 ± 0.39 [a]	15.54 ± 0.27 [a]	9.41 ± 0.44 [a]	8.42 ± 0.08 [a]	3.32 ± 0.12 [a]	—	—
2-ethyl-5-methyl Pyrazine	Thermal MR	122.0838	12.23 ± 0.10 [a]	5.60 ± 0.07 [a]	18.69 ± 0.13 [a]	27.01 ± 0.10 [a]	10.62 ± 0.11 [a]	5.98 ± 0.01 [a]	13.79 ± 0.09 [a]	6.05 ± 0.05 [a]	—	—
	HIU-MR		11.43 ± 0.08[b]	5.55 ± 0.01 [a]	18.39 ± 0.12 [a]	26.92 ± 0.04 [a]	10.80 ± 0.08 [a]	6.39 ± 0.06[b]	14.44 ± 0.12[b]	6.07 ± 0.06 [a]	—	—
2,3,5-trimethyl Pyrazine	Thermal MR	122.0838	14.16 ± 0.16 [a]	11.30 ± 0.16 [a]	4.81 ± 0.01 [a]	26.45 ± 0.07 [a]	19.08 ± 0.04 [a]	3.89 ± 0.06 [a]	12.38 ± 0.15 [a]	7.91 ± 0.07 [a]	—	—
	HIU-MR		14.22 ± 0.15 [a]	10.68 ± 0.19 [a]	4.64 ± 0.03[b]	26.65 ± 0.38 [a]	18.75 ± 0.19 [a]	3.87 ± 0.04 [a]	12.99 ± 0.14[b]	8.18 ± 0.17 [a]	—	—
3-ethyl-2,5-dimethyl Pyrazine	Thermal MR	136.0995	8.10 ± 0.13 [a]	9.32 ± 0.08 [a]	20.03 ± 0.52 [a]	15.49 ± 0.21 [a]	15.22 ± 0.14 [a]	15.58 ± 0.25 [a]	7.22 ± 0.30 [a]	6.08 ± 0.27 [a]	2.94 ± 0.19 [a]	—
	HIU-MR		7.91 ± 0.44 [a]	8.34 ± 0.46 [a]	19.84 ± 0.21 [a]	15.13 ± 0.51 [a]	15.44 ± 0.26 [a]	15.71 ± 0.26 [a]	7.96 ± 0.43 [a]	6.56 ± 0.49 [a]	3.07 ± 0.25 [a]	—
2-ethyl-3,5-dimethyl Pyrazine	Thermal MR	136.0995	13.14 ± 0.17 [a]	7.90 ± 0.17 [a]	12.51 ± 0.11 [a]	21.80 ± 0.10 [a]	16.64 ± 0.07 [a]	7.88 ± 0.11 [a]	9.31 ± 0.15 [a]	8.72 ± 0.30 [a]	2.31 ± 0.04 [a]	—
	HIU-MR		12.37 ± 0.15[b]	7.82 ± 0.15 [a]	12.65 ± 0.02 [a]	21.80 ± 0.18 [a]	16.11 ± 0.44 [a]	8.44 ± 0.14[b]	9.46 ± 0.09 [a]	8.86 ± 0.17 [a]	2.46 ± 0.08 [a]	—
tetramethyl Pyrazine	Thermal MR	136.0995	9.39 ± 0.17 [a]	12.07 ± 0.20 [a]	7.89 ± 0.06 [a]	18.55 ± 0.06 [a]	21.29 ± 0.09 [a]	9.67 ± 0.06 [a]	8.88 ± 0.15 [a]	9.22 ± 0.15 [a]	3.03 ± 0.06 [a]	—
	HIU-MR		9.64 ± 0.27 [a]	11.62 ± 0.14 [a]	7.56 ± 0.07[b]	19.00 ± 0.41 [a]	21.39 ± 0.22 [a]	9.36 ± 0.24 [a]	9.23 ± 0.18 [a]	9.29 ± 0.08 [a]	2.90 ± 0.15 [a]	—
3,5-diethyl-2-methyl Pyrazine	Thermal MR	150.1151	8.45 ± 0.14 [a]	8.70 ± 0.16 [a]	14.24 ± 0.19 [a]	16.69 ± 0.17 [a]	15.70 ± 0.15 [a]	14.23 ± 0.05 [a]	9.58 ± 0.13 [a]	7.17 ± 0.11 [a]	4.21 ± 0.04 [a]	0.99 ± 0.02 [a]
	HIU-MR		8.16 ± 0.28 [a]	8.61 ± 0.57 [a]	14.15 ± 0.25 [a]	18.00 ± 1.30 [a]	15.13 ± 0.05[b]	13.76 ± 0.17 [a]	10.19 ± 0.32 [a]	6.57 ± 0.15[b]	4.16 ± 0.30 [a]	1.23 ± 0.17 [a]
dimethyl-2-vinyl Pyrazine	Thermal MR	134.0838	5.98 ± 0.09 [a]	10.73 ± 0.06 [a]	21.65 ± 0.07 [a]	11.94 ± 0.07 [a]	17.79 ± 0.06 [a]	16.34 ± 0.15 [a]	5.59 ± 0.02 [a]	6.98 ± 0.14 [a]	2.96 ± 0.06 [a]	—
	HIU-MR		5.70 ± 0.03[b]	10.35 ± 0.05[b]	21.62 ± 0.08 [a]	11.70 ± 0.10 [a]	17.73 ± 0.03 [a]	16.60 ± 0.07[b]	5.75 ± 0.02[b]	7.52 ± 0.06[b]	3.00 ± 0.05 [a]	—

[1] The significance test of isotopomers in pyrazines generated from HIU-MR and thermal MR was conducted. Values with different letters in the same line are significantly different according to Duncan's test ($p < 0.05$).
[2] The symbol of "—" refers to not detected.

α-dicarbonyl compounds through the Strecker degradation. For 2-methyl pyrazine, it was condensed with C_2 and C_3 units from α-dicarbonyl compounds. In addition, two C_3 units as well as C_3 and C_4 units from α-dicarbonyl compounds were reacted together to generate 2,6-dimethyl pyrazine and 2-ethyl-5-methyl pyrazine, respectively.

For the pyrazines with long-length side chains, the proportion of $[M]^+$ in 2-ethyl-6-methyl pyrazine was 10.23% ± 0.07 % in the sample treated by HIU, which was significantly lower than that in thermal MR (10.88% ± 0.16%). The proportion of $[M]^+$ in 2-ethyl-3,5-dimethyl pyrazine was 11.43% ± 0.08% in the sample treated by HIU, which was significantly lower than that in thermal MR (12.23% ± 0.10%). It is also noticeable that the proportion of $[M + 5]^+$ in 2-ethyl-3,5dimethyl pyrazine was 8.44% ± 0.14% in the sample treated by HIU, which was significantly higher than that in thermal MR (7.88 ± 0.11 %). A similar find was observed in dimethyl-2-vinyl pyrazine. The proportion of $[M]^+$ was 5.70% ± 0.03% in the sample treated by HIU, which was significantly lower than that in thermal MR (5.98% ± 0.09%). The proportion of $[M + 6]^+$ and $[M + 7]^+$ in dimethyl-2-vinyl pyrazine was 5.75 ± 0.02% and 7.52 ± 0.06% in the sample treated by HIU, respectively, which was significantly higher than those in thermal MR (5.59% ± 0.02% and 6.98% ± 0.14%, respectively). Guerra and Yaylayan [25] evaluated dimerization of azomethine as an intermediate MRPs to form pyrazines in a MR model system of glyoxylic acid and glycine using CAMOLA. The 2-ethyl-3,6-dimethyl pyrazine and tetramethyl pyrazine were mainly generated through nonoxidative pathways [26].

According to the results of CAMOLA analysis, it is speculated that aldol-type condensation was promoted with the assistance of HIU, which is a conversion from pyrazines with short-length side chains to those with long-length side chains involved carbonyl compounds. As shown in Fig. 3, the unlabeled 2,6-dimethyl pyrazine, 2-methyl pyrazine, and 2-ethyl-5-methyl pyrazine would react with either labeled or unlabeled aldehydes to generate labeled 2-ethyl-6-methyl pyrazine, 2-ethyl-3,5-dimethyl pyrazine, trimethyl pyrazine, and 2-vinyl-3,5-dimethyl pyrazine. The proportion of $[M]^+$ in methanal and ethanal could be than

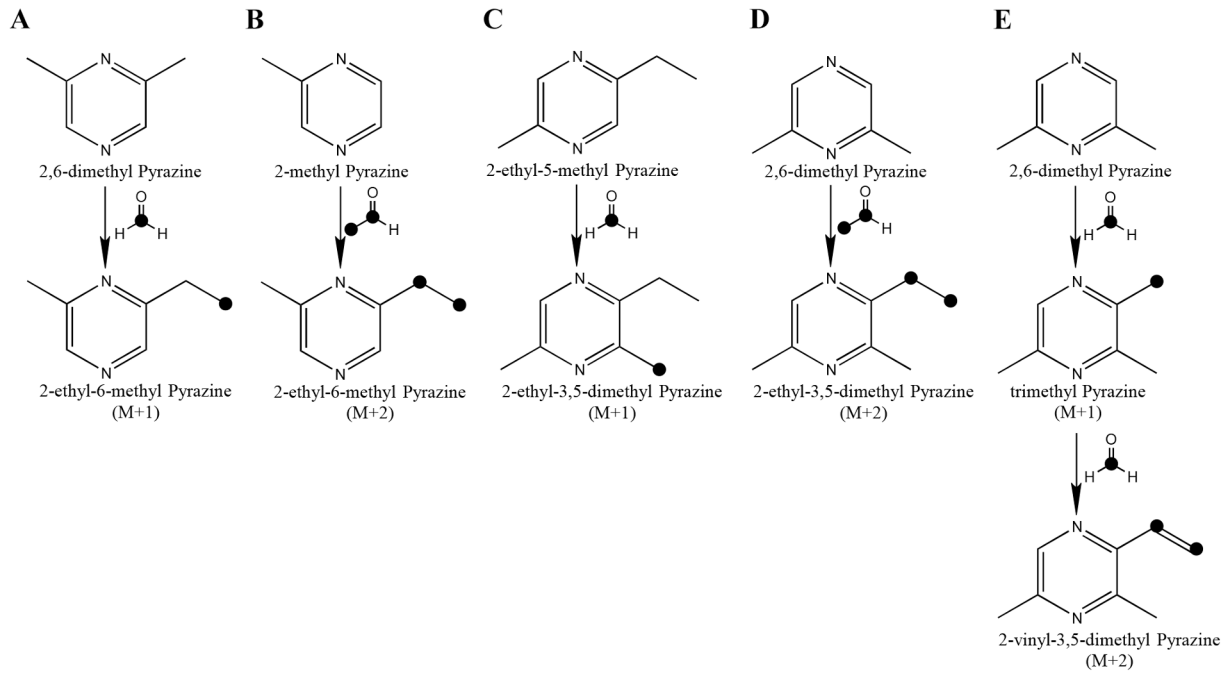

Fig. 3. Generation of isotopic pyrazines through the reactions between unlabeled pyrazines and labeled aldehydes in HIU-MR model system of D-glucose-$^{13}C_6$ and L-glycine.

Table 3
Proportion of isotopomers in OPD-derivatized α-dicarbonyl compounds generated from D-glucose-$^{13}C_6$ and L-glycine MR model systems with the assistance of HIU and thermal treatment.

α-dicarbonyl Compounds	OPD-derivatized α-dicarbonyl compounds	Type of MR	*m/z*	Proportion of labeled carbon atoms in the molecules (%)					
				M	M + 1	M + 2	M + 3	M + 4	M + 5
Glyoxal	Quinoxaline	Thermal MR	130.0525	47.06 ± 0.15 [a,1]	6.92 ± 0.08 [a]	46.02 ± 0.07 [a]	—[2]	—	—
		HIU-MR		46.79 ± 0.06 [a]	6.95 ± 0.07 [a]	46.26 ± 0.13 [a]	—	—	—
methyl Glyoxal	2-methyl Quinoxaline	Thermal MR	144.0682	45.62 ± 0.01 [a]	6.52 ± 0.02 [a]	5.14 ± 0.03 [a]	42.71 ± 0.08 [a]	—	—
		HIU-MR		45.53 ± 0.12 [a]	6.54 ± 0.07 [a]	5.16 ± 0.15 [a]	42.76 ± 0.10 [a]	—	—
2,3-Butanedione	2,3-dimethyl Quinoxaline	Thermal MR	158.0838	43.85 ± 0.64 [a]	16.79 ± 0.07 [a]	5.78 ± 0.00 [a]	18.62 ± 0.48 [a]	14.95 ± 0.09[b]	—
		HIU-MR		41.55 ± 0.39[b]	17.28 ± 0.22 [a]	5.92 ± 0.09 [a]	19.48 ± 0.20 [a]	15.74 ± 0.11 [a]	—
2,3-Pentanedione	2-ethyl-3-methyl Quinoxaline	Thermal MR	172.0995	42.66 ± 0.27 [a]	6.77 ± 0.02 [a]	1.30 ± 0.33 [a]	3.88 ± 0.01 [a]	42.69 ± 0.31 [a]	2.69 ± 0.26 [a]
		HIU-MR		41.88 ± 0.85 [a]	6.23 ± 0.57 [a]	2.19 ± 0.29 [a]	3.64 ± 0.18 [a]	43.08 ± 1.07 [a]	2.96 ± 0.27 [a]

[1] The significance test of isotopomers in OPD-derivatized α-dicarbonyl compounds generated from HIU-MR and thermal MR was conducted. Values with different letters in the same line are significantly different according to Duncan's test ($p < 0.05$).
[2] The symbol of "—" refers to not detected.

less 50% when compared with isotopomers of $[M + 1]^+$ and/or $[M + 2]^+$. For the $[M]^+$ in 2-ethyl-6-methyl pyrazine, 2-ethyl-3,5-dimethyl pyrazine, trimethyl pyrazine, and 2-vinyl-3,5-dimethyl pyrazine, all the unlabeled pyrazines could be only synthesized through aldol-type condensation between $[M]^+$ in 2,6-dimethyl pyrazine, 2-methyl pyrazine, 2-ethyl-5-methyl pyrazine, and corresponding $[M]^+$ in methanal or ethanal. The conversion rate of unlabeled pyrazines with either short-length or long-length side chains was significantly decreased. For example, the conversion rate of $[M]^+$ in 2-ethyl-6-methyl pyrazine was<10.62% from $[M]^+$ in 2,6-dimethyl pyrazine and 11.72% from $[M]^+$ in 2-methyl pyrazine. In another word, about 90% of $[M]^+$ in 2,6-dimethyl pyrazine and methyl pyrazine was converted to isotopomers in 2-ethyl-6-methyl pyrazine. Similarly, the conversion rate of $[M]^+$ in 2-ethyl-3,5-methyl pyrazine was<6.12% from $[M]^+$ in 2-ethyl-5-methyl pyrazine and 10.62% from $[M]^+$ in 2,6-dimethyl pyrazine. Therefore, the results of CAMOLA analysis clearly showed a significantly lower proportion of $[M]^+$ in the above-mentioned pyrazines compared with their corresponding isotopomers.

3.2.2. *Isotopomers in OPD-derivatized α-dicarbonyl compounds*

The proportion of isotopomers in OPD-derivatized α-dicarbonyl compounds is summarized in Table 3. Based on the results of GCMS analysis, the following intermediates were identified, i.e. quinoxaline, 2-methyl-quinoxaline, 2,3-dimethyl-quinoxaline, and 2-ethyl-3-methyl quinoxaline. The intermediate MRPs, i.e. GO, MG, 2,3-butanedione, and 2,3-bentanedione were derivatized by OPD to generate them, respectively. To confirm the origin of carbon skeleton from reactions, the CAMOLA technique combined with GCMS analysis was adopted. For

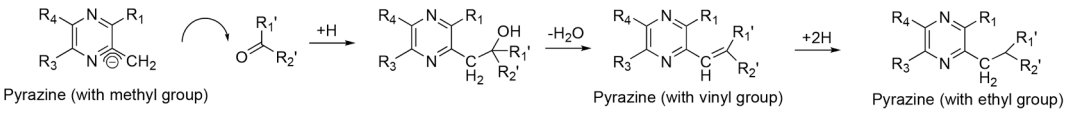

Fig. 4. Proposed aldol-type condensation in HIU-MR: a pyrazine with a methyl group would react with a carbonyl compound to synthesize a pyrazine with vinyl and furthermore, convert to a pyrazine with an ethyl group.

quinoxaline, 2-methyl-quinoxaline, and 2-ethyl-3-methyl quinoxaline, the ratio $[M]^+ : [M+2]^+ = 1:1$, $[M]^+ : [M+3]^+ = 1:1$, $[M]^+ : [M+4]^+ = 1:1$, respectively. The α-dicarbonyl compounds could be generated from decomposing Amadori compounds that lost one or more CH_2O units. Results of CAMOLA analysis showed that the additional carbon atoms mainly come from the fragments of glucose. It is noticeable that there were 6.92% of $[M+1]^+$ in quinoxaline, 6.52% of $[M+1]^+$ and 5.14% of $[M+2]^+$ in 2-methyl-quinoxaline, as well as 6.23% of $[M+1]^+$, 2.19% of $[M+2]^+$, and 3.64% of $[M+3]^+$ in 2-ethyl-3-methyl quinoxaline. For these minor isotopomers in quinoxaline, 2-methyl-quinoxaline, and 2-ethyl-3-methyl quinoxaline, these compounds could be generated between existing α-dicarbonyl compounds and labeled/unlabeled aldehydes. For quinoxaline, 2-methyl quinoxaline, and 2-ethyl-3-methyl quinoxaline, a similar isotopic distribution was observed between HIU-MR and thermal MR. These phenomena may indicate that these pyrazines originated from the same carbon skeleton.

Different from those, the ratio $[M]^+ : [M+1]^+ : [M+3]^+ : [M+4]^+ = 3:1:1:1$ in 2,3-dimethyl-quinoxaline. Results of the isotopomers distribution in 2,3-dimethyl-quinoxaline indicate a condensation between MG and glycine. Since glycine as reactants was not labeled, $[M+3]^+$ in MG or $[M+3]^+$ in glyceraldehyde could react with $[M]^+$ in glycine to generate $[M+3]^+$ in 2,3-butanedione. The condensation between $[M+3]^+$ in MG and unlabeled methanal was a potential reaction pathway to form $[M+1]^+$ in 2,3-butanedione. In addition, the proportion of $[M]^+$ in 2,3-dimethyl-quinoxaline was 41.55% ± 0.39% in the sample treated by HIU, which was significantly lower than that in thermal MR (43.85% ± 0.64%). In turn, the proportion of $[M+4]^+$ in 2,3-dimethyl-quinoxaline was 15.74% ± 0.11% in the sample treated by HIU, which was significantly higher than that in thermal MR (14.95% ± 0.09%). It could be attributed to the cleavage of D-glucose-$^{13}C_6$ promoted by HIU and thereby increasing the proportion of $[M+4]^+$ in 2,3-dimethyl-quinoxaline. Such a promotion could be mainly attributed to a high temperature and mechanically induced cleavage. The result of the significantly low proportion of $[M]^+$ in 2,3-dimethyl-quinoxaline is also in accordance with the $[M]^+$ proportion in 2-vinyl-3,5-dimethyl pyrazine. It is again indicated that 2,3-butanedione is a precursor of 2-vinyl-3,5-dimethyl pyrazine.

3.3. HIU-promoted reaction steps for synthesizing pyrazines in HIU-MR model system of D-glucose-L-glycine

Based on the results of isotopomers distribution in the pyrazines generated by HIU-MR and thermal MR, the aldol-type condensation mainly contributed to the promoted generation of pyrazines with more and long-length side chains. As proposed reaction pathway in Fig. 4, a methyl-group in a pyrazine would react with a carbonyl compound (e.g. aldehydes and ketones) to generate a vinyl-group in the pyrazine; furthermore, the vinyl-group would convert to ethyl-group in the pyrazine that eventually achieves a length extension of side chains in the pyrazines. During the HIU treatment, an extremely high-pressure condition is generated during the alteration of compression and expansion cycles [27]. Both base-catalyzed ionization of the methyl-group in pyrazine, as well as dimerization of the $-CH_2$ moiety and carbonyl compounds, show a negative volume of reaction. As a mean of extending the length of side chains in pyrazines, the aldol-type condensation favors a high pressure condition generated by the HIU [24].

The aldol-type condensation has been proved to be accelerated in a glucose-lysine MR with the assistance of high hydrostatic pressure processing (i.e. 600 MPa) at an initial pH = 10.1 [24]. Results show that the content of methyl pyrazines formation under the high-pressure condition was about 10 times lower when compared with the MR sample solution treated under the atmospheric pressure. The generation of ethyl-methyl pyrazines, however, was significantly promoted. Therefore, as speculated by the authors that the aldol-type condensation started from the methyl pyrazines to generate the pyrazines with ethyl groups. This phenomenon consists of observations in MR model systems of xylose-lysine, glucose-serine, and glucose-methionine, which also observed the promoted generation of 3-ethyl-2,5-dimethyl pyrazine and 2-ethyl-3,5-dimethyl pyrazine [11,21,28].

4. Conclusions

This study elucidated how the HIU promoted the generation of pyrazines with long-length side chains in the MR model system of D-glucose-$^{13}C_6$ and L-glycine. GCMS results of isotopomers distribution in these pyrazines indicated the HIU-promoted conversion from pyrazines with short-length side chains to those with long-length side chains involved carbonyl compounds, namely the aldol-type condensation. In addition, the CAMOLA analysis of isotopomers distribution in 2,3-dimethyl-quinoxaline indicated the promotion of D-glucose-$^{13}C_6$ cleavage with the assistance of HIU. The extremely high pressure and temperature environment generated by the HIU contributed to the promotion of both aldol-type as a high-pressure favored reaction and cleavage of glucose. Therefore, the HIU treatment has a great potential to promote the flavor generation, especially the generation of pyrazines with with high values, which have relatively high content and low odor threshold. It is also recommended to conduct further studies to verify whether such a promotion is observed in different MR model systems.

CRediT authorship contribution statement

Ruyue Zhang: Investigation, Data curation. **Yilong Zhang:** Data curation. **Yating Sun:** Visualization. **Hang Yu:** Conceptualization, Writing – original draft, Writing – review & editing, Supervision. **Fangwei Yang:** Formal analysis. **Yahui Guo:** Resources. **Yunfei Xie:** Supervision. **Weirong Yao:** Validation, Project administration.

Declaration of Competing Interest

The authors declare that they have no known competing financial interests or personal relationships that could have appeared to influence the work reported in this paper.

Acknowledgements

The following grants are gratefully acknowledged: National Nature Science Foundation of China (32001627), National Key R&D Program of China (2018YFC1602300), Key R&D Program of Jiangsu Province (BE2019362), Science and Technology Project of Market Supervision Administration of Jiangsu Province (KJ204132), the Fundamental Research Funds for the Central Universities (JUSRP11904 and JUSRP321014), and National Training Program of Innovation and Entrepreneurship for Undergraduates (202110295035Z). The first author would like to thank the financial support from High-level Innovation and Entrepreneurship Talents Introduction Program of Jiangsu Province (Su Talent Office [2019] No.20).

References

[1] L.J. van Gemert, Odour thresholds: compilations of odour threshold values in air, water and other media, Oliemans Punter (2011).

[2] H. Yu, R. Zhang, F. Yang, Y. Xie, Y. Guo, W. Yao, W. Zhou, Control strategies of pyrazines generation from Maillard reaction, Trends Food Sci. Technol. 112 (2021) 795–807.

[3] H. Yu, Y.-X. Seow, P.K.C. Ong, W. Zhou, Kinetic study of high-intensity ultrasound-assisted Maillard reaction in a model system of d-glucose and glycine, Food Chem. 269 (2018) 628–637.

[4] P.J. Thornalley, Dicarbonyl intermediates in the Maillard reaction, Ann. NY. Acad. Sci. 1043 (2005) 111–117.

[5] X.-M. Chen, D.D. Kitts, Identification and quantification of α-dicarbonyl compounds produced in different sugar-amino acid Maillard reaction model systems, Food Res. Int. 44 (2011) 2775–2782.

[6] M. Huang, A.H.P. Theng, D. Yang, H. Yang, Influence of κ-carrageenan on the rheological behaviour of a model cake flour system, LWT 136 (2021) 110324, https://doi.org/10.1016/j.lwt.2020.110324.

[7] H. Yu, Y. Liu, L.u. Li, Y. Guo, Y. Xie, Y. Cheng, W. Yao, Ultrasound-involved emerging strategies for controlling foodborne microbial biofilms, Trends Food Sci. Technol. 96 (2020) 91–101.

[8] Y.-G. Guan, J. Wang, S.-J. Yu, X.-B. Xu, S.-M. Zhu, Effects of ultrasound intensities on a glycin–maltose model system – a means of promoting Maillard reaction, Int. J. Food Sci. Tech., 45 (2010) 758-764.

[9] Y.-G. Guan, B.-S. Zhang, S.-J. Yu, X.-R. Wang, X.-B. Xu, J. Wang, Z. Han, P.-J. Zhang, H. Lin, Effects of ultrasound on a glycin–glucose model system—a means of promoting Maillard reaction, Food Bioprocess. Tech. 4 (8) (2011) 1391–1398.

[10] O.X.H. Ong, Y.-X. Seow, P.K.C. Ong, W. Zhou, High-intensity ultrasound production of Maillard reaction flavor compounds in a cysteine–xylose model system, Ultrason. Sonochem. 26 (2015) 399–407.

[11] H. Yu, M.Z.M. Keh, Y.-X. Seow, P.K.C. Ong, W. Zhou, Kinetic study of high-intensity ultrasound-assisted Maillard reaction in a model system of D-glucose and L-methionine, Food Bioprocess. Tech. 10 (11) (2017) 1984–1996.

[12] P. Schieberle, The Carbon Module Labeling (CAMOLA) Technique: A useful tool for identifying transient intermediates in the formation of maillard-type target molecules, Ann. NY. Acad. Sci. 1043 (2005) 236–248.

[13] A.-N. Yu, Z.-W. Tan, F.-S. Wang, Mechanistic studies on the formation of pyrazines by Maillard reaction between l-ascorbic acid and l-glutamic acid, LWT 50 (1) (2013) 64–71.

[14] A.-N. Yu, Z.-W. Tan, B.-A. Shi, Influence of the pH on the formation of pyrazine compounds by the Maillard reaction of L-ascorbic acid with acidic, basic and neutral amino acids, Asia-Pac. J. Chem. Eng. 7 (3) (2012) 455–462.

[15] T. Zou, J. Liu, H. Song, Y.e. Liu, Discovery of Amadori-type conjugates in a peptide Maillard Reaction and their corresponding influence on the formation of pyrazines, J. Food Sci. 83 (6) (2018) 1588–1595.

[16] J.-S. Kim, Influence of the pH and enantiomer on the antioxidant activity of Maillard reaction mixture solution in the model systems, Preventive Nutrition Food Sci. 15 (2010) 287–296.

[17] H. Yu, Q. Zhong, Y. Xie, Y. Guo, Y. Cheng, W. Yao, Kinetic study on the generation of furosine and pyrraline in a Maillard reaction model system of d-glucose and l-lysine, Food Chem. 317 (2020), 126458.

[18] S.I.F.S. Martins, M.A.J.S. van Boekel, Melanoidins extinction coefficient in the glucose/glycine Maillard reaction, Food Chem. 83 (2003) 135–142.

[19] H. Yu, Q. Zhong, Y. Liu, Y. Guo, Y. Xie, W. Zhou, W. Yao, Recent advances of ultrasound-assisted Maillard reaction, Ultrason. Sonochem. 64 (2020), 104844.

[20] X. Feng, V.K. Ng, M. Mikš-Krajnik, H. Yang, Effects of fish gelatin and tea polyphenol coating on the spoilage and degradation of myofibril in fish fillet during cold storage, Food Bioprocess. Tech. 10 (2017) 89–102.

[21] H. Yu, Y.-X. Seow, P.K. Ong, W. Zhou, Effects of high-intensity ultrasound on Maillard reaction in a model system of d-xylose and l-lysine, Ultrason. Sonochem. 34 (2017) 154–163.

[22] F. Jousse, T. Jongen, W. Agterof, S. Russell, P. Braat, Simplified kinetic scheme of flavor formation by the Maillard Reaction, J. Food Sci. 67 (2002) 2534–2542.

[23] D.S. Mottram, The Maillard Reaction: Source of flavour in thermally processed foods, in: R.G. Berger (Ed.), Flavours and Fragrances: Chemistry, Bioprocessing and Sustainability, Springer, Berlin Heidelberg, Berlin, Heidelberg, 2007, pp. 269–283.

[24] V.M. Hill, N.S. Isaacs, D.A. Ledward, J.M. Ames, Effect of high hydrostatic pressure on the volatile components of a glucose−lysine model system, J. Agr. Food Chem. 47 (1999) 3675–3681.

[25] P.V. Guerra, V.A. Yaylayan, Dimerization of azomethine ylides: An alternate route to pyrazine formation in the Maillard Reaction, J. Agr. Food Chem. 58 (2010) 12523–12529.

[26] Q. Liu, L. Chen, A.K.C. Laserna, Y. He, X. Feng, H. Yang, Synergistic action of electrolyzed water and mild heat for enhanced microbial inactivation of Escherichia coli O157:H7 revealed by metabolomics analysis, Food Control 110 (2020), 107026.

[27] Z. Gao, J. Zheng, L. Chen, Ultrasonic accelerates asparagine-glucose non-enzymatic browning reaction without acrylamide formation, Ultrason. Sonochem. 34 (2017) 626–630.

[28] H. Yu, Y.-X. Seow, P.K. Ong, W. Zhou, Generating Maillard reaction products in a model system of d-glucose and l-serine by continuous high-intensity ultrasonic processing, Innov. Food Sci. Emerg. Technol. 36 (2016) 260–268.